

UC Davis

UC Davis Previously Published Works

Title

Polarization of Λ (Λ^0) Hyperons along the Beam Direction in Au+Au Collisions at $\sqrt{s_{NN}}=200$ GeV.

Permalink

<https://escholarship.org/uc/item/42f564g6>

Journal

Physical review letters, 123(13)

ISSN

0031-9007

Authors

Adam, J
Adamczyk, L
Adams, JR
et al.

Publication Date

2019-09-01

DOI

10.1103/physrevlett.123.132301

Peer reviewed

Polarization of Λ ($\bar{\Lambda}$) hyperons along the beam direction in Au+Au collisions at $\sqrt{s_{NN}} = 200$ GeV

J. Adam,¹³ L. Adamczyk,² J. R. Adams,³⁷ J. K. Adkins,²⁸ G. Agakishiev,²⁶ M. M. Aggarwal,³⁹ Z. Ahammed,⁵⁹ I. Alekseev,^{3,33} D. M. Anderson,⁵³ R. Aoyama,⁵⁶ A. Aparin,²⁶ D. Arkhipkin,⁶ E. C. Aschenauer,⁶ M. U. Ashraf,⁵⁵ F. Atetalla,²⁷ A. Attri,³⁹ G. S. Averichev,²⁶ V. Bairathi,³⁴ K. Barish,¹⁰ A. J. Bassill,¹⁰ A. Behera,⁵¹ R. Bellwied,²⁰ A. Bhasin,²⁵ A. K. Bhati,³⁹ J. Bielcik,¹⁴ J. Bielcikova,³⁶ L. C. Bland,⁶ I. G. Bordyuzhin,³ J. D. Brandenburg,^{48,6} A. V. Brandin,³³ J. Bryslawskyj,¹⁰ I. Bunzarov,²⁶ J. Butterworth,⁴⁴ H. Caines,⁶² M. Calderón de la Barca Sánchez,⁸ D. Cebra,⁸ I. Chakaberia,^{27,6} P. Chaloupka,¹⁴ B. K. Chan,⁹ F.-H. Chang,³⁵ Z. Chang,⁶ N. Chankova-Bunzarova,²⁶ A. Chatterjee,⁵⁹ S. Chattopadhyay,⁵⁹ J. H. Chen,¹⁸ X. Chen,⁴⁷ J. Cheng,⁵⁵ M. Cherney,¹³ W. Christie,⁶ H. J. Crawford,⁷ M. Csanád,¹⁶ S. Das,¹¹ T. G. Dedovich,²⁶ I. M. Deppner,¹⁹ A. A. Derevschikov,⁴¹ L. Didenko,⁶ C. Dilks,⁴⁰ X. Dong,²⁹ J. L. Drachenberg,¹ J. C. Dunlop,⁶ T. Edmonds,⁴² N. Elsey,⁶¹ J. Engelage,⁷ G. Eppley,⁴⁴ R. Esha,⁵¹ S. Esumi,⁵⁶ O. Evdokimov,¹² J. Ewigeleben,³⁰ O. Eyser,⁶ R. Fatemi,²⁸ S. Fazio,⁶ P. Federic,³⁶ J. Fedorisin,²⁶ Y. Feng,⁴² P. Filip,²⁶ E. Finch,⁵⁰ Y. Fisyak,⁶ L. Fulek,² C. A. Gagliardi,⁵³ T. Galatyuk,¹⁵ F. Geurts,⁴⁴ A. Gibson,⁵⁸ K. Gopal,²² D. Grosnick,⁵⁸ A. Gupta,²⁵ W. Guryn,⁶ A. I. Hamad,²⁷ A. Hamed,⁵ J. W. Harris,⁶² L. He,⁴² S. Heppelmann,⁸ S. Heppelmann,⁴⁰ N. Herrmann,¹⁹ L. Holub,¹⁴ Y. Hong,²⁹ S. Horvat,⁶² B. Huang,¹² H. Z. Huang,⁹ S. L. Huang,⁵¹ T. Huang,³⁵ X. Huang,⁵⁵ T. J. Humanic,³⁷ P. Huo,⁵¹ G. Igo,⁹ W. W. Jacobs,²³ C. Jena,²² A. Jentsch,⁵⁴ Y. Ji,⁴⁷ J. Jia,^{6,51} K. Jiang,⁴⁷ S. Jowzaee,⁶¹ X. Ju,⁴⁷ E. G. Judd,⁷ S. Kabana,²⁷ S. Kagamaster,³⁰ D. Kalinkin,²³ K. Kang,⁵⁵ D. Kapukchyan,¹⁰ K. Kauder,⁶ H. W. Ke,⁶ D. Keane,²⁷ A. Kechechyan,²⁶ M. Kelsey,²⁹ Y. V. Khyzhniak,³³ D. P. Kikoła,⁶⁰ C. Kim,¹⁰ T. A. Kinghorn,⁸ I. Kisel,¹⁷ A. Kisiel,⁶⁰ M. Kocan,¹⁴ L. Kochenda,³³ L. K. Kosarzewski,¹⁴ L. Kramarik,¹⁴ P. Kravtsov,³³ K. Krueger,⁴ N. Kulathunga Mudiyansele,²⁰ L. Kumar,³⁹ R. Kunnawalkam Elayavalli,⁶¹ J. H. Kwasizur,²³ R. Lacey,⁵¹ J. M. Landgraf,⁶ J. Lauret,⁶ A. Lebedev,⁶ R. Lednicky,²⁶ J. H. Lee,⁶ C. Li,⁴⁷ W. Li,⁴⁹ W. Li,⁴⁴ X. Li,⁴⁷ Y. Li,⁵⁵ Y. Liang,²⁷ R. Licenik,¹⁴ T. Lin,⁵³ A. Lipiec,⁶⁰ M. A. Lisa,³⁷ F. Liu,¹¹ H. Liu,²³ P. Liu,⁵¹ P. Liu,⁴⁹ T. Liu,⁶² X. Liu,³⁷ Y. Liu,⁵³ Z. Liu,⁴⁷ T. Ljubicic,⁶ W. J. Llope,⁶¹ M. Lomnitz,²⁹ R. S. Longacre,⁶ S. Luo,¹² X. Luo,¹¹ G. L. Ma,⁴⁹ L. Ma,¹⁸ R. Ma,⁶ Y. G. Ma,⁴⁹ N. Magdy,¹² R. Majka,⁶² D. Mallick,³⁴ S. Margetis,²⁷ C. Markert,⁵⁴ H. S. Matis,²⁹ O. Matonoha,¹⁴ J. A. Mazer,⁴⁵ K. Meehan,⁸ J. C. Mei,⁴⁸ N. G. Minaev,⁴¹ S. Mioduszewski,⁵³ D. Mishra,³⁴ B. Mohanty,³⁴ M. M. Mondal,²⁴ I. Mooney,⁶¹ Z. Moravcova,¹⁴ D. A. Morozov,⁴¹ Md. Nasim,⁹ K. Nayak,¹¹ J. M. Nelson,⁷ D. B. Nemes,⁶² M. Nie,⁴⁸ G. Nigmatkulov,³³ T. Niida,⁶¹ L. V. Nogach,⁴¹ T. Nonaka,¹¹ G. Odyniec,²⁹ A. Ogawa,⁶ K. Oh,⁴³ S. Oh,⁶² V. A. Okorokov,³³ B. S. Page,⁶ R. Pak,⁶ Y. Panebratsev,²⁶ B. Pawlik,³⁸ D. Pawlowska,⁶⁰ H. Pei,¹¹ C. Perkins,⁷ R. L. Pintér,¹⁶ J. Pluta,⁶⁰ J. Porter,²⁹ M. Posik,⁵² N. K. Pruthi,³⁹ M. Przybycien,² J. Putschke,⁶¹ A. Quintero,⁵² S. K. Radhakrishnan,²⁹ S. Ramachandran,²⁸ R. L. Ray,⁵⁴ R. Reed,³⁰ H. G. Ritter,²⁹ J. B. Roberts,⁴⁴ O. V. Rogachevskiy,²⁶ J. L. Romero,⁸ L. Ruan,⁶ J. Rusnak,³⁶ O. Rusnakova,¹⁴ N. R. Sahoo,⁴⁸ P. K. Sahu,²⁴ S. Salur,⁴⁵ J. Sandweiss,⁶² J. Schambach,⁵⁴ W. B. Schmidke,⁶ N. Schmitz,³¹ B. R. Schweid,⁵¹ F. Seck,¹⁵ J. Seger,¹³ M. Sergeeva,⁹ R. Seto,¹⁰ P. Seyboth,³¹ N. Shah,⁴⁹ E. Shahaliev,²⁶ P. V. Shanmuganathan,³⁰ M. Shao,⁴⁷ F. Shen,⁴⁸ W. Q. Shen,⁴⁹ S. S. Shi,¹¹ Q. Y. Shou,⁴⁹ E. P. Sichtermann,²⁹ S. Siejka,⁶⁰ R. Sikora,² M. Simko,³⁶ J. Singh,³⁹ S. Singha,²⁷ D. Smirnov,⁶ N. Smirnov,⁶² W. Solyst,²³ P. Sorensen,⁶ H. M. Spinka,⁴ B. Srivastava,⁴² T. D. S. Stanislaus,⁵⁸ M. Stefaniak,⁶⁰ D. J. Stewart,⁶² M. Strikhanov,³³ B. Stringfellow,⁴² A. A. P. Suaide,⁴⁶ T. Sugiura,⁵⁶ M. Sumera,³⁶ B. Summa,⁴⁰ X. M. Sun,¹¹ Y. Sun,⁴⁷ Y. Sun,²¹ B. Surrow,⁵² D. N. Svirida,³ P. Szymanski,⁶⁰ A. H. Tang,⁶ Z. Tang,⁴⁷ A. Taranenko,³³ T. Tarnowsky,³² J. H. Thomas,²⁹ A. R. Timmins,²⁰ D. Tlusty,¹³ T. Todoroki,⁶ M. Tokarev,²⁶ C. A. Tomkiel,³⁰ S. Trentalange,⁹ R. E. Tribble,⁵³ P. Tribedy,⁶ S. K. Tripathy,²⁴ O. D. Tsai,⁹ B. Tu,¹¹ Z. Tu,⁶ T. Ullrich,⁶ D. G. Underwood,⁴ I. Upsal,^{48,6} G. Van Buren,⁶ J. Vanek,³⁶ A. N. Vasiliev,⁴¹ I. Vassiliev,¹⁷ F. Videbæk,⁶ S. Vokal,²⁶ S. A. Voloshin,⁶¹ F. Wang,⁴² G. Wang,⁹ P. Wang,⁴⁷ Y. Wang,¹¹ Y. Wang,⁵⁵ J. C. Webb,⁶ L. Wen,⁹ G. D. Westfall,³² H. Wieman,²⁹ S. W. Wissink,²³ R. Witt,⁵⁷ Y. Wu,²⁷ Z. G. Xiao,⁵⁵ G. Xie,¹² W. Xie,⁴² H. Xu,²¹ N. Xu,²⁹ Q. H. Xu,⁴⁸ Y. F. Xu,⁴⁹ Z. Xu,⁶ C. Yang,⁴⁸ Q. Yang,⁴⁸ S. Yang,⁶ Y. Yang,³⁵ Z. Yang,¹¹ Z. Ye,⁴⁴ Z. Ye,¹² L. Yi,⁴⁸ K. Yip,⁶ I. -K. Yoo,⁴³ H. Zbroszczyk,⁶⁰ W. Zha,⁴⁷ D. Zhang,¹¹ L. Zhang,¹¹ S. Zhang,⁴⁷ S. Zhang,⁴⁹ X. P. Zhang,⁵⁵ Y. Zhang,⁴⁷ Z. Zhang,⁴⁹ J. Zhao,⁴² C. Zhong,⁴⁹ C. Zhou,⁴⁹ X. Zhu,⁵⁵ Z. Zhu,⁴⁸ M. Zurek,²⁹ and M. Zyzak¹⁷

(STAR Collaboration)

¹Abilene Christian University, Abilene, Texas 79699

²AGH University of Science and Technology, FPACS, Cracow 30-059, Poland

³Alikhanov Institute for Theoretical and Experimental Physics, Moscow 117218, Russia

- ⁴Argonne National Laboratory, Argonne, Illinois 60439
⁵American University of Cairo, Cairo, Egypt
⁶Brookhaven National Laboratory, Upton, New York 11973
⁷University of California, Berkeley, California 94720
⁸University of California, Davis, California 95616
⁹University of California, Los Angeles, California 90095
¹⁰University of California, Riverside, California 92521
¹¹Central China Normal University, Wuhan, Hubei 430079
¹²University of Illinois at Chicago, Chicago, Illinois 60607
¹³Creighton University, Omaha, Nebraska 68178
¹⁴Czech Technical University in Prague, FNSPE, Prague 115 19, Czech Republic
¹⁵Technische Universität Darmstadt, Darmstadt 64289, Germany
¹⁶Eötvös Loránd University, Budapest, Hungary H-1117
¹⁷Frankfurt Institute for Advanced Studies FIAS, Frankfurt 60438, Germany
¹⁸Fudan University, Shanghai, 200433
¹⁹University of Heidelberg, Heidelberg 69120, Germany
²⁰University of Houston, Houston, Texas 77204
²¹Huzhou University, Huzhou, Zhejiang 313000
²²Indian Institute of Science Education and Research, Tirupati 517507, India
²³Indiana University, Bloomington, Indiana 47408
²⁴Institute of Physics, Bhubaneswar 751005, India
²⁵University of Jammu, Jammu 180001, India
²⁶Joint Institute for Nuclear Research, Dubna 141 980, Russia
²⁷Kent State University, Kent, Ohio 44242
²⁸University of Kentucky, Lexington, Kentucky 40506-0055
²⁹Lawrence Berkeley National Laboratory, Berkeley, California 94720
³⁰Lehigh University, Bethlehem, Pennsylvania 18015
³¹Max-Planck-Institut für Physik, Munich 80805, Germany
³²Michigan State University, East Lansing, Michigan 48824
³³National Research Nuclear University MEPhI, Moscow 115409, Russia
³⁴National Institute of Science Education and Research, HBNI, Jatni 752050, India
³⁵National Cheng Kung University, Tainan 70101
³⁶Nuclear Physics Institute of the CAS, Rez 250 68, Czech Republic
³⁷Ohio State University, Columbus, Ohio 43210
³⁸Institute of Nuclear Physics PAN, Cracow 31-342, Poland
³⁹Panjab University, Chandigarh 160014, India
⁴⁰Pennsylvania State University, University Park, Pennsylvania 16802
⁴¹NRC "Kurchatov Institute", Institute of High Energy Physics, Protvino 142281, Russia
⁴²Purdue University, West Lafayette, Indiana 47907
⁴³Pusan National University, Pusan 46241, Korea
⁴⁴Rice University, Houston, Texas 77251
⁴⁵Rutgers University, Piscataway, New Jersey 08854
⁴⁶Universidade de São Paulo, São Paulo, Brazil 05314-970
⁴⁷University of Science and Technology of China, Hefei, Anhui 230026
⁴⁸Shandong University, Qingdao, Shandong 266237
⁴⁹Shanghai Institute of Applied Physics, Chinese Academy of Sciences, Shanghai 201800
⁵⁰Southern Connecticut State University, New Haven, Connecticut 06515
⁵¹State University of New York, Stony Brook, New York 11794
⁵²Temple University, Philadelphia, Pennsylvania 19122
⁵³Texas A&M University, College Station, Texas 77843
⁵⁴University of Texas, Austin, Texas 78712
⁵⁵Tsinghua University, Beijing 100084
⁵⁶University of Tsukuba, Tsukuba, Ibaraki 305-8571, Japan
⁵⁷United States Naval Academy, Annapolis, Maryland 21402
⁵⁸Valparaiso University, Valparaiso, Indiana 46383
⁵⁹Variable Energy Cyclotron Centre, Kolkata 700064, India
⁶⁰Warsaw University of Technology, Warsaw 00-661, Poland
⁶¹Wayne State University, Detroit, Michigan 48201
⁶²Yale University, New Haven, Connecticut 06520
- (Dated: May 29, 2019)

The Λ ($\bar{\Lambda}$) hyperon polarization along the beam direction has been measured for the first time in Au+Au collisions at $\sqrt{s_{NN}} = 200$ GeV. The polarization dependence on the hyperons' emission angle relative to the second-order event plane exhibits a sine modulation, indicating a quadrupole pattern

of the vorticity component along the beam direction. The polarization is found to increase in more peripheral collisions, and shows no strong transverse momentum (p_T) dependence at $p_T > 1$ GeV/ c . The magnitude of the signal is about five times smaller than those predicted by hydrodynamic and multiphase transport models; the observed phase of the emission angle dependence is also opposite to these model predictions. In contrast, blast-wave model calculations reproduce the modulation phase measured in the data and capture the centrality and transverse momentum dependence of the signal once the model is required to reproduce the azimuthal dependence of the Gaussian source radii measured via the Hanbury-Brown and Twiss intensity interferometry technique.

PACS numbers: 25.75.-q, 25.75.Ld

The properties of deconfined partonic matter, the quark-gluon plasma, have been explored in heavy-ion collisions at the Relativistic Heavy Ion Collider (RHIC) [1–4] and the Large Hadron Collider [5–7]. The matter created in non-central heavy-ion collisions should exhibit rotational motion in order to conserve the initial angular momentum carried by the two colliding nuclei. The direction of the angular momentum is perpendicular to the reaction plane, as defined by incoming beam and the impact parameter vector. It was predicted [8, 9] that such a spinning motion of the matter would lead to a net spin polarization of particles produced in the collisions due to spin-orbit coupling. Hyperons are natural candidates to explore this phenomenon since in the parity violating weak decays of the hyperons the momentum vector of the decay baryon is highly correlated with the hyperon spin. In such decays the angular distribution of the daughter baryons is given by:

$$\frac{dN}{d\cos\theta^*} \propto 1 + \alpha_H P_H \cos\theta^*, \quad (1)$$

where α_H is the hyperon decay parameter, P_H is the hyperon polarization, and θ^* is the angle between the polarization vector and the direction of the daughter baryon momentum in the hyperon rest frame.

The Solenoidal Tracker at RHIC (STAR) Collaboration has observed positive polarizations of Λ hyperons along the orbital angular momentum in Au+Au collisions for collision energies of $\sqrt{s_{NN}} = 7.7 - 200$ GeV [10, 11]. This polarization is evidence for the creation of the most vortical fluid ever observed, with vorticities of the order of $\omega \sim 10^{22} \text{ s}^{-1}$. These results open new opportunities for a better understanding of the dynamics and properties of the matter created in heavy-ion collisions.

The spin polarization of hyperons along the orbital angular momentum of the entire system is referred to as the *global* polarization, meaning a net spin alignment along a globally defined direction. However, the vorticity and, consequently, the particle polarization may vary for different regions of the fluid due to anisotropic flow, energy deposits from jet quenching, density fluctuations, etc. The detailed structure of the vorticity fields may be complicated and the resulting particle polarization can depend on the particle transverse momentum and the azimuthal angle relative to the reaction plane, or even exhibit toroidal structures [12–15].

Anisotropic flow, characterized by the Fourier coefficients of the particle azimuthal distribution in the transverse plane, has been extensively studied in heavy-ion collisions and was found to be well described by hydrodynamic calculations [16, 17]. Nontrivial velocity fields describing transverse anisotropic flow should lead to a vorticity component along the beam direction dependent on the azimuthal angle relative to the reaction plane [13, 14]. The observation of the large second-order coefficients, a.k.a. elliptic flow, in mid-central collisions indicates significantly stronger expansion in the reaction plane direction compared to that out-of-plane, which might lead to a quadrupole structure in the z -component of vorticity as illustrated in Fig. 1. Experimental measurements of such a component are the main goal of this analysis.

The beam direction component of the polarization arising from vorticity due to elliptic flow is expected to be more sensitive to later times from flow development in the system evolution [18], unlike the global polarization that originates mostly from the initial velocity fields. It might also have different sensitivity to the relaxation time needed for the conversion of the vorticity into particle polarization. Therefore, it is of great interest to study the polarization along the beam direction for further understanding of the role of the vorticity in heavy-ion collisions and possibly to answer these questions. In this Letter, we report the beam direction component of polarization for Λ and $\bar{\Lambda}$ hyperons in Au+Au collisions at $\sqrt{s_{NN}} = 200$ GeV. The results are presented as functions of the collision centrality and hyperons' transverse momentum (p_T).

The dataset for this analysis was collected in 2014 by the STAR detector during the period of Au+Au collisions at $\sqrt{s_{NN}} = 200$ GeV. Charged-particle tracks were measured in the time projection chamber (TPC) [19], which covers the full azimuth and a pseudorapidity range of $-1 < \eta < 1$. The collision vertices were reconstructed using the measured charged-particle tracks. Events were selected to have the collision vertex position within 6 cm of the center of the TPC in the beam direction and within 2 cm in the radial direction with respect to the beam center. In addition, the difference between the vertex positions along the beam direction determined by the TPC and the vertex position detectors (VPD) [20] located at forward and backward rapidities ($4.24 < |\eta| < 5.1$) was

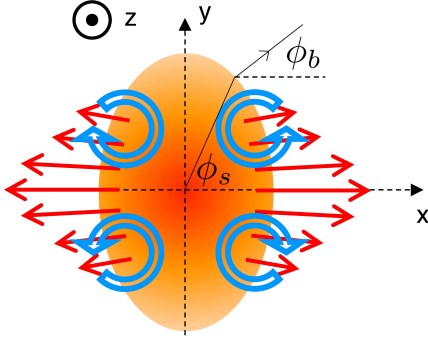


FIG. 1. (Color online) A sketch illustrating the system created in a non-central heavy-ion collision viewed in the transverse plane (x-y), showing stronger in-plane expansion (solid arrows) and expected vorticities (open arrows). In this figure the colliding beams are oriented along the z-axis and the x-z plane defines the reaction plane. See text for explanations of ϕ_s and ϕ_b .

required to be less than 3 cm to suppress pileup events. These selection criteria yielded about one billion minimum bias events, where the minimum bias trigger required hits of both VPDs and the zero-degree calorimeters [21] located at $|\eta| > 6.3$.

The collision centrality was determined from the measured multiplicity of charged particles within $|\eta| < 0.5$ and a Monte-Carlo Glauber simulation [22]. The second-order event plane (Ψ_2) as an experimental estimate of the reaction plane was determined by the charged-particle tracks within the transverse momentum range of $0.15 < p_T < 2$ GeV/c and $0.1 < |\eta| < 1$:

$$\Psi_2^{\text{obs}} = \tan^{-1} \left(\frac{\sum_i w_i \sin(2\phi_i)}{\sum_i w_i \cos(2\phi_i)} \right), \quad (2)$$

where ϕ_i and w_i are the azimuthal angle and p_T of the i^{th} particle in the event. The resolution of the measured plane Ψ_2^{obs} defined as $\text{Res}(\Psi_2) = \langle \cos 2(\Psi_2^{\text{obs}} - \Psi_2) \rangle$ was estimated with the two-subevent method [23], where the two subevents were taken from $0.1 < |\eta| < 1$. In mid-central collisions the event plane resolution peaks at ~ 0.76 .

Charged-particle tracks reconstructed with the TPC were selected to have good quality by requiring the following conditions. The number of hit points used in the track reconstruction was required to be larger than 15. The ratio of the number of hit points used to the maximum possible number of TPC space points for that trajectory was required to be larger than 0.52. Tracks within $0.15 < p_T < 10$ GeV/c and $|\eta| < 1$ that passed through the track selections above were used to reconstruct Λ hyperons. In order to reconstruct Λ and $\bar{\Lambda}$, the decay channels of $\Lambda \rightarrow p + \pi^-$ and $\bar{\Lambda} \rightarrow \bar{p} + \pi^+$, corresponding to $(63.9 \pm 0.5)\%$ of all decays [24], were utilized. The ionization energy loss dE/dx in the TPC and the time of flight

information of the particles from the time-of-flight detector [25] were used to select daughter pions and protons. Cuts on decay topology, such as a distance of the closest approach (DCA) between the trajectory of Λ ($\bar{\Lambda}$) candidates and the primary vertex, DCA between the two daughters, and decay length of Λ ($\bar{\Lambda}$) candidates were applied to reduce the combinatoric background. Additional details about the Λ ($\bar{\Lambda}$) reconstruction can be found in Ref. [11].

The longitudinal component of the polarization can be measured by projecting the polarization onto the beam direction:

$$P_z = \frac{\langle \cos \theta_p^* \rangle}{\alpha_H \langle \cos^2 \theta_p^* \rangle}, \quad (3)$$

where θ_p^* is the polar angle of the daughter proton in the Λ ($\bar{\Lambda}$) rest frame and $\langle \rangle$ represents an average over Λ ($\bar{\Lambda}$) candidates in an event and then an average over all events. The decay parameter α_H is set to be $\alpha_\Lambda = -\alpha_{\bar{\Lambda}} = 0.642 \pm 0.013$ [24, 26]. If the detector has perfect acceptance and efficiency, $\langle \cos^2 \theta_p^* \rangle$ leads to $1/3$. In this study $\langle \cos^2 \theta_p^* \rangle$ was extracted from the data in order to account for pseudorapidity dependent detector acceptance effects. This term was found to be close to $1/3$ for all centralities but showed a systematic decrease for lower track p_T . To extract the signal $\langle \cos \theta_p^* \rangle$, two techniques were used: the event plane method and the invariant mass method as described in Ref. [11]. In the event plane method, $\langle \cos \theta_p^* \rangle$ was measured as a function of azimuthal angle of Λ ($\bar{\Lambda}$) relative to Ψ_2 . The average polarization along the beam direction is expected to be zero due to symmetry. Effects due to detector acceptance and inefficiencies are removed by subtracting the azimuthal average of $\langle \cos \theta_p^* \rangle$ from each azimuthal bin i of Λ azimuthal angle: $\langle \cos \theta_p^* \rangle_i^{\text{sub}} = \langle \cos \theta_p^* \rangle_i - \sum_i^{\text{nbin}} \langle \cos \theta_p^* \rangle_i / n_{\text{bin}}$.

Figure 2 shows $\langle \cos \theta_p^* \rangle_i^{\text{sub}}$ of Λ and $\bar{\Lambda}$ as a function of azimuthal angle relative to Ψ_2 for the 20%–60% centrality bin. The solid lines indicate the fit results to the function $p_0 + 2p_1 \sin(2\phi - 2\Psi_2)$, where p_0 and p_1 are fit parameters. The data are consistent with a sine structure for both Λ and $\bar{\Lambda}$ as expected from the elliptic flow. In the invariant mass method, the second-order Fourier sine coefficient of P_z , $p_1 = \langle P_z \sin(2\phi - 2\Psi_2) \rangle$, was measured as a function of the invariant mass. Following the same procedure as described in Ref. [11], the sine coefficient was directly extracted. The extracted coefficient in both methods was divided by $\text{Res}(\Psi_2)$ to account for the finite event plane resolution. The invariant mass method was used to calculate the sine coefficient of P_z and the event plane method was used to cross-check and provide an estimate of the systematic uncertainty.

The systematic uncertainties were estimated by variation of the topological cuts ($< 2\%$), comparing the results from two methods for signal extraction (5%) as mentioned above, using different subevents ($-1 < \eta < -0.5$

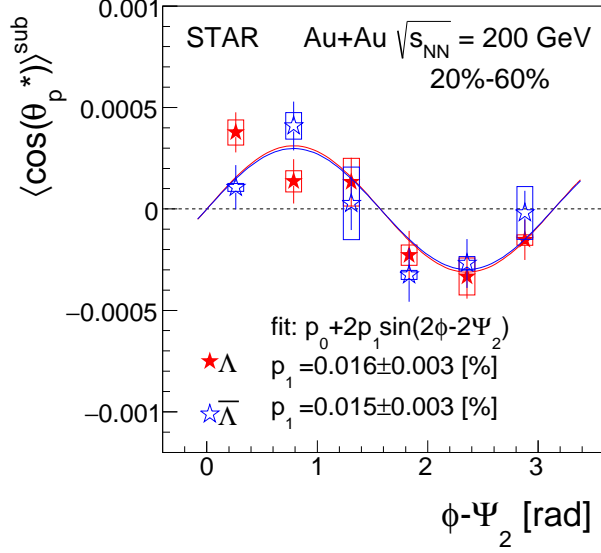


FIG. 2. (Color online) $\langle \cos \theta_p^* \rangle$ of Λ and $\bar{\Lambda}$ hyperons as a function of azimuthal angle ϕ relative to the second-order event plane Ψ_2 for 20%-60% centrality bin in Au+Au collisions at $\sqrt{s_{NN}} = 200$ GeV. Open boxes show the systematic uncertainties and $\langle \rangle^{\text{sub}}$ denotes the subtraction of the acceptance effect (see text). Solid lines show the fit with the sine function shown inside the figure. Note that the data are not corrected for the event plane resolution.

and $0.5 < \eta < 1$) for Ψ_2 determination ($< 11\%$), and estimates of the possible background contribution to the signal (4.3%). The numbers are for mid-central collisions. Also the uncertainty from the decay parameter is accounted for (2% for Λ and 9.6% for $\bar{\Lambda}$, see Ref. [11] for the detail). We further studied the effect of a possible self-correlation between the particles used for the Λ ($\bar{\Lambda}$) reconstruction and the event plane by explicitly removing the daughter particles from the event plane calculation in Eq. (2). There was no significant difference between the results. The Λ and $\bar{\Lambda}$ reconstruction efficiencies were estimated using GEANT [28] simulations of the STAR detector [19]. The correction is found to lower mean values of the P_z sine coefficient by $\sim 10\%$ in peripheral collisions and increases up to $\sim 50\%$ in central collisions, although the variations are within statistical uncertainties. No significant difference was observed between Λ and $\bar{\Lambda}$ as expected. Therefore, results from both samples were combined to reduce statistical uncertainties.

Figure 3 presents the centrality dependence of the second Fourier sine coefficient $\langle P_z \sin(2\phi - 2\Psi_2) \rangle$. The increase of the signal with decreasing centrality is likely due to increasing elliptic flow contributions in peripheral collisions. We note that, unlike elliptic flow, the polarization does disappear in the most central collisions, where the elliptic flow is still significant due to initial density fluctuations. Because of large uncertainties in periph-

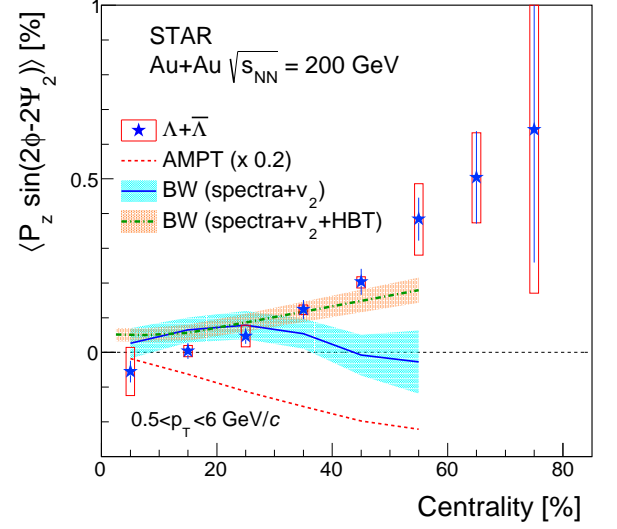


FIG. 3. (Color online) The second Fourier sine coefficient of the polarization of Λ and $\bar{\Lambda}$ along the beam direction as a function of the collision centrality in Au+Au collisions at $\sqrt{s_{NN}} = 200$ GeV. Open boxes show the systematic uncertainties. Dotted line shows the AMPT calculation [27] scaled by 0.2 (no p_T selection). Solid and dot-dashed lines with the bands show the blast-wave (BW) model calculation for $p_T = 1$ GeV/c with Λ mass (see text for details).

eral collisions, it is not clear whether the signal continues to increase or levels off. The results are compared to a multiphase transport (AMPT) model [27] as shown with the dotted line. The AMPT model predicts the opposite phase of the modulations and overestimates the magnitude. The blast-wave model study is discussed later.

Since the elliptic flow also depends on p_T as well as on the centrality, the polarization may have p_T dependence. Figure 4 shows the sine coefficients of P_z as a function of the hyperon transverse momentum. No significant p_T dependence is observed for $p_T > 1$ GeV/c, and the statistical precision of the single data point for $p_T < 1$ GeV/c is not enough to allow for definitive conclusions about the low p_T dependence. In the hydrodynamic model calculation [14], the sine coefficient of P_z increases in magnitude with p_T but shows the opposite sign to the data.

As shown in Figs. 3 and 4, the hydrodynamic and AMPT models predict the opposite sign in the sine coefficient of the polarization and their magnitudes differ from the data roughly by a factor of 5. The reason of this sign difference is under discussion in the community. However, the sign change may be due to the relation between azimuthal anisotropy and spatial anisotropy at freeze-out [13]. There could be contributions from the kinematic vorticity originating from the elliptic flow as well as from the temporal gradient of temperatures at the time of hadronization [14]. A recent calculation us-

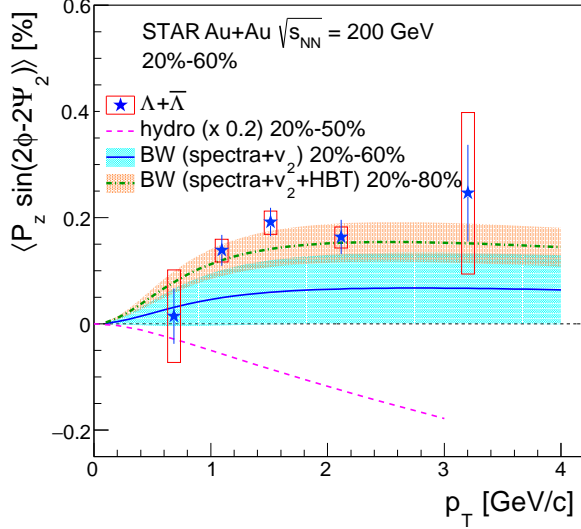


FIG. 4. (Color online) The second Fourier sine coefficient of the longitudinal polarization of Λ and $\bar{\Lambda}$ hyperons as a function of p_T for 20%-60% centrality bin in Au+Au collisions at $\sqrt{s_{NN}} = 200$ GeV. Open boxes show the systematic uncertainties. Magenta dashed line shows the hydrodynamic model calculation [14] scaled by 0.2. Solid and dot-dashed lines with the bands show the blast-wave (BW) model calculations with Λ mass.

ing the chiral kinetic approach predicts the same sign as the data [29]. The model accounts for the transverse component of the vorticity, resulting in axial charge currents. Note that both the hydrodynamic and transport models calculate local vorticity at freeze-out and convert it to the polarization assuming local thermal equilibrium of the spin degrees of freedom, while the chiral kinetic approach takes into account nonequilibrium effects but does not consider a contribution from the temperature gradient which is a main source of P_z in the hydrodynamic model.

These models indicate that the contribution from the kinematic vorticity to P_z is negligible or opposite in the sign to the naive expectation from the elliptic flow. In order to estimate the contribution from the kinematic vorticity we employed the blast-wave model (BW) [30–32]. Following Ref. [32] we parameterize the system velocity field at freeze-out with temperature (T) and transverse flow rapidity (ρ) defined as $\rho = \tilde{r}[\rho_0 + \rho_2 \cos(2\phi_b)]$. Here ρ_0 and ρ_2 are the maximal radial expansion rapidity and its azimuthal modulation, \tilde{r} is the relative distance to the edge of the source, and ϕ_b defines the direction of the local velocity as indicated in Fig. 1. The source shape, assumed to be elliptical in the transverse plane, is parameterized by the R_y and R_x radii. Boost invariance is assumed. Two fits to the data are performed: in one only spectra and elliptic flow of π , K, and $p(\bar{p})$ are fit; the sec-

ond fit [33] also includes azimuthal-angle-dependence of the pion Gaussian source radii at freeze-out as measured via Hanbury-Brown and Twiss (HBT) intensity interferometry. The average longitudinal vorticity is calculated according to the following formula:

$$\langle \omega_z \sin(2\phi) \rangle = \frac{\int d\phi_s \int r dr I_2(\alpha_t) K_1(\beta_t) \omega_z \sin(2\phi_b)}{\int d\phi_s \int r dr I_0(\alpha_t) K_1(\beta_t)} \quad (4)$$

$$\omega_z = \frac{1}{2} \left(\frac{\partial u_y}{\partial x} - \frac{\partial u_x}{\partial y} \right), \quad (5)$$

where the integration is over the transverse cross-sectional area of the source, u_μ is a four-vector of the local flow velocity [32], ϕ_s is the azimuth of the production point (see Fig. 1 for the relation to ϕ_b), $\alpha_t = p_T/T \sinh \rho$, $\beta_t = m_T/T \cosh \rho$; I_n and K_1 are the modified Bessel functions. Assuming a local thermal equilibrium, the longitudinal component of the polarization is estimated as $P_z \approx \omega_z/(2T)$. The uncertainties shown for the BW model calculations corresponds to 1 σ variation in the model parameters. See Ref. [34] for more details.

The BW calculations are compared to the data in Figs. 3 and 4. From central to mid-central collisions both BW calculations show positive sine coefficients which are compatible in both sign and magnitude to the measurement, although the BW model is based on a very simple picture of the freeze-out condition. It was shown in Ref. [13] that the vorticity in the BW model has the effects of the velocity field anisotropy (ρ_2/ρ_0) and the spacial source anisotropy (R_y/R_x) contributing with opposite signs, which can explain a strong sensitivity of the BW model predictions in the peripheral collisions to the inclusions of the HBT radii.

We have presented the first measurements of the longitudinal component of the polarization for Λ and $\bar{\Lambda}$ hyperons in Au+Au collisions at $\sqrt{s_{NN}} = 200$ GeV. Finite signals of a quadrupole modulation of both Λ and $\bar{\Lambda}$ polarization along the beam direction are observed and found to be qualitatively consistent with the expectation from the vorticity component along the beam direction due to the elliptic flow. The results exhibit a strong centrality dependence with increasing magnitude as the collision centrality becomes more peripheral. No significant p_T dependence is observed above $p_T > 1$ GeV/c. A drop-off of the signal is hinted at for $p_T < 1$ GeV/c. The data were compared to calculations from hydrodynamic and AMPT models, both of which show the opposite phase of the modulation and overpredict the magnitude of the polarization. This might indicate incomplete thermal equilibration of the spin degrees of freedom for the beam direction component of the vorticity/polarization, as it develops later in time compared to the global polarization. On the other hand, the blast-wave model calculations are much closer to the data, even more so when the azimuthally sensitive HBT results along with the p_T spectra and v_2 are included in the model fit. The blast-wave model predicts the correct phase of P_z modulation

and a similar p_T dependence; the version with HBT radii included in the fit also reasonably describes the centrality dependence. These results together with the results of the global polarization may provide information on the relaxation time needed to convert the vorticity to particle polarization. Further theoretical and experimental studies are needed for better understanding.

We thank the RHIC Operations Group and RCF at BNL, the NERSC Center at LBNL, and the Open Science Grid consortium for providing resources and support. This work was supported in part by the Office of Nuclear Physics within the U.S. DOE Office of Science, the U.S. National Science Foundation, the Ministry of Education and Science of the Russian Federation, National Natural Science Foundation of China, Chinese Academy of Science, the Ministry of Science and Technology of China and the Chinese Ministry of Education, the National Research Foundation of Korea, Czech Science Foundation and Ministry of Education, Youth and Sports of the Czech Republic, Hungarian National Research, Development and Innovation Office (FK-123824), New National Excellency Programme of the Hungarian Ministry of Human Capacities (UNKP-18-4), Department of Atomic Energy and Department of Science and Technology of the Government of India, the National Science Centre of Poland, the Ministry of Science, Education and Sports of the Republic of Croatia, RosAtom of Russia and German Bundesministerium für Bildung, Wissenschaft, Forschung und Technologie (BMBF) and the Helmholtz Association.

-
- [1] J. Adams *et al.* (STAR Collaboration), “Experimental and Theoretical Challenges in the Search for the Quark Gluon Plasma: The STAR Collaboration’s Critical Assessment of the Evidence from RHIC Collisions,” *Nucl. Phys. A* **757**, 102 (2005).
 - [2] K. Adcox *et al.* (PHENIX Collaboration), “Formation of dense partonic matter in relativistic nucleus-nucleus collisions at RHIC: Experimental evaluation by the PHENIX collaboration,” *Nucl. Phys. A* **757**, 184 (2005).
 - [3] B. B. Back *et al.* (PHOBOS Collaboration), “The PHOBOS Perspective on Discoveries at RHIC,” *Nucl. Phys. A* **757**, 28 (2005).
 - [4] I. Arsene *et al.* (BRAHMS Collaboration), “Quark Gluon Plasma and Color Glass Condensate at RHIC? The perspective from the BRAHMS experiment,” *Nucl. Phys. A* **757**, 1 (2005).
 - [5] K. Aamodt *et al.* (ALICE Collaboration), “Suppression of charged particle production at large transverse momentum in central Pb-Pb collisions at $\sqrt{s_{NN}} = 2.76$ TeV,” *Phys. Lett. B* **696**, 30–39 (2011).
 - [6] S. Chatrchyan *et al.* (CMS Collaboration), “Observation and studies of jet quenching in PbPb collisions at $\sqrt{s_{NN}} = 2.76$ TeV,” *Phys. Rev. C* **84**, 024906 (2011).
 - [7] G. Aad *et al.* (ATLAS Collaboration), “Observation of a centrality-dependent dijet asymmetry in lead-lead collisions at $\sqrt{s_{NN}} = 2.76$ TeV with the ATLAS detector at the LHC,” *Phys. Rev. Lett.* **105**, 252303 (2010).
 - [8] Z. T. Liang and X. N. Wang, “Globally Polarized Quark-Gluon Plasma in Noncentral A+A Collisions,” *Phys. Rev. Lett.* **94**, 102301 (2005), [Erratum: *Phys. Rev. Lett.* **96**, 039901 (2006)].
 - [9] S. A. Voloshin, “Polarized secondary particles in unpolarized high energy hadron-hadron collisions?” (2004), [arXiv:nucl-th/0410089 \[nucl-th\]](#).
 - [10] L. Adamczyk *et al.* (STAR Collaboration), “Global Λ hyperon polarization in nuclear collisions,” *Nature* **548**, 62 (2017).
 - [11] J. Adam *et al.* (STAR Collaboration), “Global polarization of Λ hyperons in Au+Au collisions at $\sqrt{s_{NN}} = 200$ GeV,” *Phys. Rev. C* **98**, 014910 (2018).
 - [12] B. Betz, M. Gyulassy, and G. Torrieri, “Polarization probes of vorticity in heavy ion collisions,” *Phys. Rev. C* **76**, 044901 (2007).
 - [13] S. A. Voloshin, “Vorticity and particle polarization in heavy ion collisions (experimental perspective),” *17th International Conference on Strangeness in Quark Matter (SQM 2017) Utrecht, the Netherlands, July 10-15, 2017*, (2017), [10.1051/epjconf/201817107002](#), [EPJ Web Conf.17,10700(2018)].
 - [14] F. Becattini and Iu. Karpenko, “Collective longitudinal polarization in relativistic heavy-ion collisions at very high energy,” *Phys. Rev. Lett.* **120**, 012302 (2018).
 - [15] L.-G. Pang, H. Petersen, Q. Wang, and X.-N. Wang, “Vortical Fluid and Λ Spin Correlations in High-Energy Heavy-Ion Collisions,” *Phys. Rev. Lett.* **117**, 192301 (2016).
 - [16] S. A. Voloshin, A. M. Poskanzer, and R. Snellings, “Collective phenomena in non-central nuclear collisions,” *Landolt-Bornstein* **23**, 293 (2010).
 - [17] U. Heinz and R. Snellings, “Collective flow and viscosity in relativistic heavy-ion collisions,” *Ann. Rev. Nucl. Part. Sci.* **63**, 123 (2013).
 - [18] D. Teaney and L. Yan, “Triangularity and dipole asymmetry in relativistic heavy ion collisions,” *Phys. Rev. C* **83**, 064904 (2011).
 - [19] M. Anderson *et al.*, “The STAR time projection chamber: A unique tool for studying high multiplicity events at RHIC,” *Nucl. Instrum. Meth. A* **499**, 659 (2003).
 - [20] W. J. Llope *et al.*, “The STAR Vertex Position Detector,” *Nucl. Instrum. Meth. A* **759**, 23 (2014).
 - [21] C. Adler, A. Denisov, E. Garcia, M. Murray, H. Strobele, and S. White, “The RHIC zero degree calorimeters,” *Nucl. Instrum. Meth. A* **461**, 337 (2001).
 - [22] L. Adamczyk *et al.* (STAR Collaboration), “Inclusive charged hadron elliptic flow in Au+Au collisions at $\sqrt{s_{NN}} = 7.7$ –39 GeV,” *Phys. Rev. C* **86**, 054908 (2012).
 - [23] A. M. Poskanzer and S. A. Voloshin, “Methods for analyzing anisotropic flow in relativistic nuclear collisions,” *Phys. Rev. C* **58**, 1671 (1998).
 - [24] C. Patrignani *et al.* (Particle Data Group), “Review of Particle Physics,” *Chin. Phys. C* **40**, 100001 (2016).
 - [25] W. J. Llope, “Multigap RPCs in the STAR experiment at RHIC,” *Nucl. Instrum. Meth. A* **661**, S110 (2012).
 - [26] Recent studies [35, 36] show 12%-17% higher α_Λ than Ref. [24]. Therefore the measured polarization could be smaller by that amount.
 - [27] X.-L. Xia, H. Li, Z.-B. Tang, and Q. Wang, “Probing vorticity structure in heavy-ion collisions by local Λ polarization,” *Phys. Rev. C* **98**, 024905 (2018).

- [28] R. Brun, F. Bruyant, M. Maire, A. C. McPherson, and P. Zancarini, “GEANT3,” (1987).
- [29] Y. Sun and C. M. Ko, “Azimuthal angle dependence of the longitudinal spin polarization in relativistic heavy ion collisions,” *Phys. Rev. C* **99**, 011903 (2019).
- [30] E. Schnedermann, J. Sollfrank, and U. W. Heinz, “Thermal phenomenology of hadrons from 200A GeV S+S collisions,” *Phys. Rev. C* **48**, 2462 (1993).
- [31] C. Adler *et al.* (STAR Collaboration), “Identified particle elliptic flow in Au + Au collisions at $\sqrt{s_{NN}} = 130$ GeV,” *Phys. Rev. Lett.* **87**, 182301 (2001).
- [32] F. Retiere and M. A. Lisa, “Observable implications of geometrical and dynamical aspects of freeze-out in heavy ion collisions,” *Phys. Rev. C* **70**, 044907 (2004).
- [33] J. Adams *et al.* (STAR Collaboration), “Pion interferometry in Au+Au collisions at $\sqrt{s_{NN}} = 200$ GeV,” *Phys. Rev. C* **71**, 044906 (2005).
- [34] A. Dobrin, R. Bertens, T. Niida, and S. A. Voloshin, in preparation.
- [35] M. Ablikim *et al.* (BESIII Collaboration), “Polarization and Entanglement in Baryon-Antibaryon Pair Production in Electron-Positron Annihilation,” *Nature Physics* (2019), 10.1038/s41567-019-0494-8.
- [36] D. G. Ireland, M. Dring, D. I. Glazier, J. Haidenbauer, M. Mai, R. Murray-Smith, and D. Rnchen, “Kaon Photoproduction and the Λ Decay Parameter α_- ,” (2019), [arXiv:1904.07616](https://arxiv.org/abs/1904.07616).